Response of a maglev vehicle moving on a series of guideways with differential settlement

J.D. Yau*

Department of Architecture, Tamkang University, Taipei 10620, Taiwan

Abstract

The objective of this study is to investigate the dynamic response of a maglev (magnetically levitated) vehicle traveling over a series of guideway girders undergoing ground support settlement. The maglev vehicle is simulated as a rigid car body supported by a rigid levitation frame using a uniformly distributed spring–dashpot system, and the guideway unit is modeled as a series of simple beams with identical span. To carry out the interaction dynamics of maglev vehicle/guideway system, this study adopts a PI (proportional-integral) controller with *constant* tuning gains based on Ziegler–Nicholas (Z–N) method to regulate the electromagnetic forces between the magnetic-wheels and guide-rail. For the inclusion of support movements, the total response of the simple beam is decomposed into two parts: the *static* response due to support settlement and the *dynamic* component caused by inertia effect of beam vibration. Once the *static* displacement for a simple beam undergoing vertical support movements is derived, the remaining dynamic response of the maglev vehicle/guideway system is solved by Galerkin's method and computed by an iterative approach using Newmark's finite difference formulas. Numerical studies indicate that the increase in levitation gap for a maglev vehicle may result in larger vehicle's response, but the response of the maglev vehicle with *smaller* air gap will be significantly amplified at higher speeds once ground settlement appears at the guideway supports.
© 2009 Elsevier Ltd. All rights reserved.

1. Introduction

Compared with the traditional railway system using wheel/track contact technology, maglev (magnetically levitated) system can offer several advantages in reducing noise, vibration, energy consumption, waste gas discharge, and maintenance costs for its absence of contact with guideway [1]. Thus, maglev transport system features its potential development in a region with fast growing demand of intercity travel, such as the Shanghai maglev transport system.

In the past two decades, numerous researchers have contributed their efforts to dynamic problems for a maglev vehicle running on a flexible guideway [2–6,20]. Concerning the dynamic interaction response of maglev trains traveling over a two-span guideway at high speeds, Cai et al. [2] pointed out that a

*Tel.: +886 2 33933833x8210; fax: +886 2 23959041.

E-mail address: jdyau@mail.tku.edu.tw

concentrated-load vehicle model might give rise to larger response on both guideway deflections and vehicle accelerations than a distributed-load vehicle model. In addition, Cai and Chen [3] provided a literature review for various aspects of the dynamic characteristics, magnetic suspension systems, vehicle stability, suspension control laws of maglev/guideway coupling systems. To investigate the vibration behavior of a maglev vehicle moving on a flexible guideway, Zheng et al. [4,5] developed two kinds of vehicle/guideway coupling models with controllable magnetic suspension systems to observe the phenomena of divergence, flutter, and collision on the dynamic stability of a maglev vehicle traveling on a flexible guideway. Zhao and Zhai [6] simulated a TR06 carriage as a ten-degree-of-freedom (10-dof) vehicle model with a rigid car body supported by four sets of equivalent bogie systems to investigate the vertical random response and ride quality of a maglev vehicle traveling on elevated guideways. However, to the author's knowledge, relatively little research attention so far seems to conduct the influence of ground settlement on interaction response of a maglev vehicle crossing a series of guideways, especially concerning the maglev vehicle with different levitation gaps.

Differential ground settlement at guideway supports, generally speaking, is one of key issues for running safety and operation of maglev systems, the reason of support settlement can be attributed to the following: earthquake shaking, different soil conditions below bridge foundations, loading capacity of sub-soil in construction site, and compaction of earth fill. For a maglev system, any of these factors may result in guide track sinking and distorting in rail geometry, which are harmful to the ride quality and maneuverability of moving maglev vehicles. In this study, a maglev vehicle is simulated as a rigid car body connected with a rigid levitation frame using a uniformly distributed spring–dashpot system. The guideway system is modeled as a series of simply supported beams with identical properties. To resolve the dynamic problem for a simple beam undergoing vertical support settlement, the total response of the beam is decomposed into two parts: the *static* response due to support settlement and the *dynamic* component caused by inertial effect of beam vibration [7,8]. An exact solution for *static* displacement is presented by exerting the support displacements on the simple beam statically. To explore the influence of ground settlement on interaction response of the maglev vehicle/guideway system, this study adopts an optimal PI controller with *constant* tuning gains based on Ziegler–Nicholas (Z–N) tuning rule [9–11] to regulate the electromagnetic forces exerting on the moving maglev vehicle. Then the two sets of differential equations associated with the equations of control electromagnetic forces for the maglev vehicle/guideway system are computed using an iterative approach with Newmark's finite difference scheme [12]. Numerical studies indicate that the effect of differential settlement is generally small on the guideway girder response, but it can significantly amplify the dynamic response of the moving maglev vehicle with small air gap at higher speeds. Such a fact should be taken into account in the design stage for a maglev transport system if its guideway route has to cross the region with potential land subsidence.

2. Governing equations of motion

With the advance of magnetic levitation technology in transport, two kinds of maglev technologies in practical applications have been developed: (1) the electrodynamic suspension (EDS) with repulsive mode [1,13,14]; (2) the electromagnetic suspension (EMS) with attractive mode. The EDS system suspends a train above its guide-rail using magnetic repulsive forces to take the train off the U-shaped guideway. One feature of EDS-type maglev trains is that its magnetic levitation is workable only at high speeds [1]. On the other hand, the EMS system can lift a train up using attractive forces by the magnets beneath a guide-rail at any speed, which is the major difference from the EDS system.

From the numerical results presented by Cai et al. [2], they pointed out that a distributed-load vehicle model behaves better than a concentrated-load model in both responses of guideway and vehicles, which indicates that the vehicle supported with multiple magnets may have better ride quality. For this reason, the maglev vehicle supported with multiple magnetic wheels is employed to conduct the dynamic behavior of the maglev vehicle/guideway system in this study. As shown in Fig. 1, an EMS-type maglev vehicle is traveling over a series of guideways. Considering the dominant factor for vibration behaviors of the maglev vehicle/guideway interaction system, only vertical motions of the dynamic model are concerned in this study [2].

The following are the assumptions adopted for the maglev vehicle/guideway system: (1) The guideway system is modeled as a series of simply supported beams with identical properties and the beam is idealized as
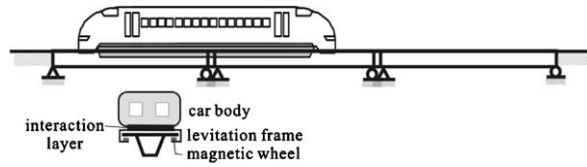
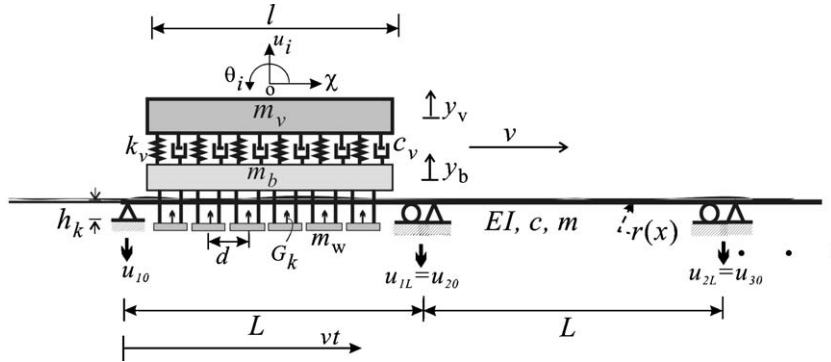Fig. 1. A series of guideways traveled by a maglev vehicle.

Fig. 2. Model of a maglev vehicle running on a series of simple beams.

a linear elastic Bernoulli–Euler beam with uniform section; (2) the maglev vehicle is simulated as a *rigid* double-beam system, in which the car body and levitation frame are modeled as two rigid parallel beams connected by an interaction layer (secondary suspension system) using a uniformly distributed spring–dashpot system (see Fig. 2); (3) allowable levitation gap (h) at the magnetic wheel should not contact with the guide-rail, i.e., $h > 0$; (4) the magnetic wheels in the maglev system are regarded as a series of equal-distant concentrated masses attached to the rigid levitation frame; (5) the effect of guideway–soil interaction is supposed to be insignificant; (6) the time delay between the input voltage and output current on the maglev suspension system is negligible.

As shown in Fig. 2, a maglev vehicle supported by multiple magnet wheels with equal-intervals (d) is passing through a series of simple beams at constant speed v. Here, we shall use the following symbols to denote the properties depicted in the schematic diagram of Fig. 2: m is the distributed mass of the beam, c is the damping coefficient, EI is the flexural rigidity, l is the car length, m_w is the lumped mass of magnetic wheel, m_b is the distributed mass of the levitation frame, m_v is the distributed mass of the car body, and $(u_i, \theta_i)|_{i=b,v}$ is the midpoint displacement and rotation components of the rigid-double beam system. Here, the subscripts b and v are denoted as the rigid lower (levitation frame) and upper (car body) beams for the maglev vehicle model, respectively. With the inclusion of ground settlement at guideway supports, one can formulate the equation of motion for the jth guideway girder carrying a moving maglev vehicle suspended by multiple magnetic forces G_k as follows:

$$m\ddot{u}_j + c\dot{u}_j + EIu_j'''' = \sum_{k=1}^{K}[G_k(i_k, h_k)\varphi_j(x, t)], \tag{1}$$

and

$$\varphi_j(x, t) = \delta(x - x_k)\left[H\left(t - t_k - \frac{(j-1)L}{v}\right) - H\left(t - t_k - \frac{jL}{v}\right)\right], \tag{2}$$

together with the following non-homogeneous boundary conditions due to vertical support movements:

$$u_j(0, t) = u_{j0}, \quad u_j(L, t) = u_{jL},$$

$$EIu_j''(0, t) = EIu_j''(L, t) = 0, \tag{3}$$

where $(\bullet)' = \partial(\bullet)/\partial x$, $(\dot{\bullet}) = \partial(\bullet)/\partial t$, $u_j(x,t)$ is the vertical deflection of the jth span, L is the span length, K is the number of magnetic wheel-sets attached to the rigid levitation frame, $\delta(\bullet)$ is the Dirac's delta function, $H(t)$ is the unit step function, $k = 1,2,3,\dots,K$th moving magnetic wheel on the beam, $t_k = (k-1)d/v$ is the arrival time of the kth magnetic wheel into the beam, x_k is the position of the kth magnetic wheel on the guideway, u_{j0} is the vertical settlement at $x = 0$ of the jth beam, and u_{jL} is the vertical settlement at $x = L$ of the jth beam. Considering the equilibrium of a differential element shown in Fig. 3 for a vibrating rigid double-beam system, the equations of motion for the element suspended by the kth magnetic force G_k are given by

$$m_v \ddot{y}_v + c_v(\dot{y}_v - \dot{y}_b) + k_v(y_v - y_b) = 0,$$

$$(m_b + m_w\delta(\chi - \chi_k))\ddot{y}_b + c_v(\dot{y}_b - \dot{y}_v) + k_v(y_b - y_v) = -p_0 + G_k(i, h). \qquad (4)$$

Here, χ is the horizontal coordinate along the longitudinal axis of the vehicle model, y_b is the vertical displacement of the rigid lower beam at χ, y_v is the vertical displacement of the rigid upper beam at position χ, $p_0 = (m_v + m_b + m_w\delta(\chi - \chi_k))g$ is the lumped weight acting on the kth magnetic wheel, and g is the gravity acceleration. It is noted that the coordinate origin "o" is located at the midpoint of the ith rigid-beam in Fig. 3. Considering the nature of *rigid* double-beam system, the vertical displacements (y_b, y_v) at position χ are, respectively, given by

$$y_b = u_b + \chi\theta_b, \quad y_v = u_v + \chi\theta_v, \quad -l/2 \leqslant \chi \leqslant l/2, \qquad (5)$$

where u_b the midpoint displacement of the rigid lower beam, u_v the midpoint displacement of the rigid upper beam, θ_b the rigid pitching rotation of the lower beam, and θ_v the rigid pitching rotation of the upper beam. In addition, the control electromagnetic force between the kth lumped magnetic wheel and the guideway is given by [1,15,20]

$$G_k(i_k, h_k) = K_0\left(\frac{i_k(t)}{h_k(t)}\right)^2, \qquad (6)$$

where $K_0 = \mu_0 N_0^2 A_0/4$ is the coupling factor [1,15], μ_0 is the vacuum permeability, N_0 is the number of turns of the magnet windings, A_0 is the pole face area, $i(t) = i_0 + \iota(t)$ is the control current, $\iota(t)$ is the deviation of control current, $h_k(t) = h_0 + y_v(t) - u_j(x_k) + r(x_k)$ is the levitation gap, $r(x)$ is the irregularity of guideway, and (i_0, h_0) is the desired control current and levitation gap around a specified nominal operating point for the maglev wheels at static equilibrium. From the electromagnetic force expressed in Eq. (6), the motion-dependent nature of magnetic force plays a key role to resolve the dynamic problem of maglev vehicle–guideway interaction tuned by a maglev system. From the equilibrium condition of the *rigid* double-beam system, we can express Eqs. (4) in potential form using the principle of virtual displacement as follows:

$$\int_{-l/2}^{l/2} [(m_b + m_w\delta(\chi - x_k))\ddot{y}_b + c_v(\dot{y}_b - \dot{y}_v) + k_v(y_b - y_v)]\delta y_b \, d\chi = \int_{-l/2}^{l/2} [(-p_0 + G_k(i_k, h_k))\delta(\chi - \chi_k)]\delta y_b \, d\chi, \qquad (7)$$
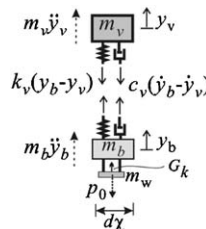

Fig. 3. Fee body diagram for a differential element of the rigid double-beam system.

Thus, after integration and some variational derivation, Eq. (7) can be further transformed into the following equations of motion for a 4-dof maglev vehicle:

Lower beam (levitation frame):

$$(m_b + Km_w/l)\ddot{u}_b + c_v(\dot{u}_b - \dot{u}_v) + k_v(u_b - u_v) = -f_0 + \frac{1}{l}\sum_{k=1}^{K} G_k(i_k, h_k),$$

$$I_{bT}\ddot{\theta}_v + \frac{l^2}{12}[c_v(\dot{\theta}_v - \dot{\theta}_b) + k_v(\theta_v - \theta_b)] = \sum_{k=1}^{K}[G_k(i_k, h_k)d_k], \qquad (8a,b)$$

Upper beam (car body):

$$m_v\ddot{u}_v + c_v(\dot{u}_v - \dot{u}_b) + k_v(u_v - u_b) = 0,$$

$$I_v\ddot{\theta}_b + \frac{l^2}{12}[c_v(\dot{\theta}_b - \dot{\theta}_v) + k_v(\theta_b - \theta_v)] = 0, \qquad (9a,b)$$

in which d_k is the distance of the kth magnetic wheel to the midpoint of the lower beam, $I_b = m_b l^2/12$ is the moment of inertia for the rigid levitation frame, $I_{bT} = I_b + \sum_{k=1}^{K} m_w d_k^2$, $I_v = m_v l^2/12$ is the moment of inertia for the rigid car body, and $f_0 = (m_v + m_b + Km_w/l)g$ is the average weight per unit length. Eq. (8) represents the equations of motion for the levitation frame interacting with the guideway and Eq. (9) for the rigid car body. Besides, from the condition of static equilibrium for the suspended maglev vehicle, one can obtain the following *static* electromagnetic force at the kth magnetic wheel from Eq. (8a):

$$G_k(i_0, h_0) = \kappa_0\left(\frac{i_0}{h_0}\right)^2 = \frac{f_0 l}{K}, \qquad (10)$$

where the coupling factor $\kappa_0 = f_0 l(h_0/i_0)^2/K$.

3. Equation of control for the maglev suspension system

By the theory of electromagnetic circuits, the electromagnetic equation of magnet current and control voltage for the kth magnetic wheel in the magnetic suspension system is given by [14,15]

$$\Gamma_0\frac{\mathrm{d}(i_k/h_k)}{\mathrm{d}t} + R_0 i_k = V_k, \qquad (11)$$

where $\Gamma_0 = 2\kappa_0$ is the initial inductance of the coil winding the suspension magnet, R_0 is the coil resistance of electronic circuit, and V_k is the control voltage. To conduct the dynamic response of maglev vehicle/guideway system subject to ground settlement, an on-board PI controller with *constant* tuning gains is employed for the moving maglev vehicle. On the other hand, the control voltage V_k can be expressed using PI tuning algorithm as [10,11,20]

$$V_k = K_p e_k + K_i \int_0^t e_k \,\mathrm{d}t, \qquad (12)$$

where K_p is the proportional gain and K_i the integral gain. Let us adopt the variable transformation as $\gamma_k = i_k/h_k$, and the error function of $e_k = i_0/h_0 - i_k/h_k = \gamma_0 - \gamma_k$ in the control process. Then substituting Eq. (12) into Eq. (11) and differentiating this equation with respect to time, after some mathematical manipulation, one can achieve the following differential equation for control error function:

$$\Gamma_0\ddot{e}_k + (K_p + R_0 h_k)\dot{e}_k + (K_i + R_0\dot{h}_k)e_k - R_0\gamma_0(\dot{u}_b + d_k\dot{\theta}_b) = -R_0\gamma_0(\dot{u}_j - \dot{r})|_{x=x_k}. \qquad (13)$$

With the aid of control error function e_k and $\gamma_0 = i_0/h_0$ defined previously, the equations of motion in Eqs. (8) and (9) for a maglev vehicle are rewritten as

$$(m_b + Km_w/l)\ddot{u}_b + c_v(\dot{u}_b - \dot{u}_v) + k_v(u_b - u_v) + \frac{2f_0}{\gamma_0 K}\sum_{k=1}^{K} e_k = \frac{f_0}{K\gamma_0^2}\sum_{k=1}^{K} e_k^2,$$

$$I_{bT}\ddot{\theta}_v + \frac{l^2}{12}[c_v(\dot{\theta}_v - \dot{\theta}_b) + k_v(\theta_v - \theta_b)] + \frac{2f_0 l}{\gamma_0 K}\sum_{k=1}^{K}(d_k e_k) = \frac{f_0 l}{K\gamma_0^2}\sum_{k=1}^{K}(d_k e_k^2),$$

$$m_v\ddot{u}_v + c_v(\dot{u}_v - \dot{u}_b) + k_v(u_v - u_b) = 0,$$

$$I_v\ddot{\theta}_b + \frac{l^2}{12}[c_v(\dot{\theta}_b - \dot{\theta}_v) + k_v(\theta_b - \theta_v)] = 0. \tag{14}$$

Combining Eqs. (13) and (14) yields the following equation of motion for the present maglev vehicle model:

$$[m_c]\{\ddot{u}_v\} + [c_c]\{\dot{u}_v\} + [k_c]\{u_v\} = \{f_v\} \tag{15}$$

of which the displacement vector $\{u_v\}$, force vector $\{f_v\}$, and structural matrices of $[k_c]$, $[c_c]$, and $[m_c]$ have been given in Appendix 1.

4. Method of solution

As the beam equation shown in Eqs. (1) and (3), it is a differential equation associated with non-homogeneous boundary conditions. The total deflection response $u_j(x,t)$ can be decomposed into two parts: the *static* displacement $U_j(x)$ and the *dynamic* deflection $u_{dj}(x,t)$ [7,8], or

$$u_j(x, t) = U_j(x) + u_{dj}(x, t). \tag{16}$$

Here, $U_j(x)$ represents the *static* displacement caused by *relative* support settlement, and $u_{dj}(x,t)$ the *dynamic* deflection due to inertia effect of beam vibration [7]. By using the static decomposition concept, substituting Eq. (16) into Eq. (1), and discarding all the dynamic terms and external loads, the static equation of motion in terms of the static displacement $U_j(x)$ is 0:

$$EI\frac{\partial^4 U_j}{\partial x^4} = 0. \tag{17}$$

And the static response $U_j(x)$ in Eq. (17) has to satisfy the following *non-homogeneous* boundary conditions in Eqs. (3):

$$U_j(0) = u_{j0}, \quad U_j(L) = u_{jL},$$

$$EIU_j''(0) = EIU_j''(L) = 0. \tag{18}$$

Solving the forth-order differential equation in Eq. (17) associated with the boundary conditions of Eqs. (18) yields

$$U_j = u_{j0} + (u_{jL} - u_{j0}) \times x/L. \tag{19}$$

The *static* displacement shown in Eq. (19) represents the *rigid body* displacements of the *j*th beam undergoing differential support movements. Furthermore, introducing Eqs. (16) and (19) into Eq. (1), the equation of motion for the *j*th simple beam is converted into the following vibration equation in terms of *dynamic* deflection $u_{dj}(x,t)$ as

$$m\ddot{u}_{dj} + c\dot{u}_{dj} + EIu_{dj}'''' = \sum_{k=1}^{K}[G_k(i_k, h_k)\varphi_j(x, t)]. \tag{20}$$

Since the static displacement $U_j(x)$ in Eq. (19) has satisfied the boundary conditions with vertical support movements shown in Eqs. (3), the introduction of Eqs. (16) and (19) into Eqs. (3) yields the following

homogeneous boundary conditions for the dynamic deflection $u_{dj}(x,t)$:

$$u_{dj}(0,t) = u_{dj}(L,t) = 0,$$

$$EIu''_{dj}(0,t) = EIu''_{dj}(L,t) = 0. \tag{21}$$

Obviously, the response of *dynamic* deflection $u_{dj}(x,t)$ in Eq. (20) associated with the homogeneous boundary conditions in Eqs. (21) can be solved by Galerkin's method [16–18] and computed by Newmark's method [12] in the time domain. According to the homogeneous boundary conditions shown in Eqs. (21), the dynamic deflection (u_{dj}) of a simple beam can be approximated by [16,20]:

$$u_{dj}(x,t) = \sum_{n=1} q_{jn}(t) \sin\frac{n\pi x}{L}, \tag{22}$$

where $q_{jn}(t)$ means the generalized coordinate associated with the nth assumed mode of the jth span. First, multiplying both sides of Eq. (20) with respect to the variation of the dynamic deflection (δu_{dj}), and then integrating the equation over the beam length L, one can obtain the following generalized equation of motion for the nth *dynamic* system of the jth beam:

$$m\ddot{q}_{jn} + c\dot{q}_{jn} + k_n q_{jn} = p_{jn}, \tag{23}$$

where $k_n = EI(n\pi/L)^4$ is the generalized stiffness, and the generalized magnetic force is

$$p_{jn} = \sum_{k=1}^{K}[G_k(i_k,h_k)\psi_{jn}(\varpi_n,t)], \tag{24}$$

$$\psi_{jn}(\varpi_n,t) = \sin \varpi_n(t-t_k)\left[H(t-t_k-\frac{(j-1)L}{v}) - H\left(t-t_k-\frac{jL}{v}\right)\right], \tag{25}$$

with $\varpi_n = n\pi v/L$ [16–18].

5. Applications of the incremental-iterative approach

Because of the motion-dependent nature of electromagnetic forces, the nonlinear dynamic analysis of the maglev vehicle/guideway system needs to be solved by iterative method. The procedure of incremental-iterative dynamic analysis conventionally involves three phases: *predictor*, *corrector*, and *equilibrium checking* [19]. Details concerning the incremental-iterative procedure for nonlinear dynamic analysis of vehicle–bridge interaction are available in Refs. [19,20]. Fig. 4 shows the analysis flow chat to carry out the nonlinear dynamic analysis for the interaction response of maglev vehicle/guideway system including ground support settlement. It is noted that (1) the total guideway deflection response in the flow chart have taken the static displacement due to support movements into account for finding the corresponding beam deflection under the kth magnetic wheel running over the guideway girder; (2) the structure matrices in Appendix 1 for the dynamic interaction between the moving maglev vehicle and the guideway should be updated at each iteration; (3) the root mean square β_{tol} of the sum of unbalanced forces for the maglev vehicle/guideway interaction system, i.e.,

$$\beta_{\text{tol}} = \left[\sum_{k=1...}(\Delta f_{vk,t+\Delta t}^{i-1})^2 + \sum_{n=1...}(\Delta p_{n,t+\Delta t}^{i-1})^2\right]^{1/2} \tag{26}$$

is larger than a preset tolerance, say 10^{-3}, iteration for removing the unbalanced forces involving the two phases of predictor and corrector should be repeated. Here, $\Delta p_{n,t+\Delta t}^{i-1}$ is the unbalanced force between the external force $p_{n,t+\Delta t}^{i-1}$ and the effective internal forces $f_{n,t+\Delta t}^{i-1}$ for the nth generalized system at the ith iteration of time $t + \Delta t$, and $\Delta f_{vk,t+\Delta t}^{i-1}$ is the unbalanced force for the kth maglev wheels to lift up the maglev vehicle.
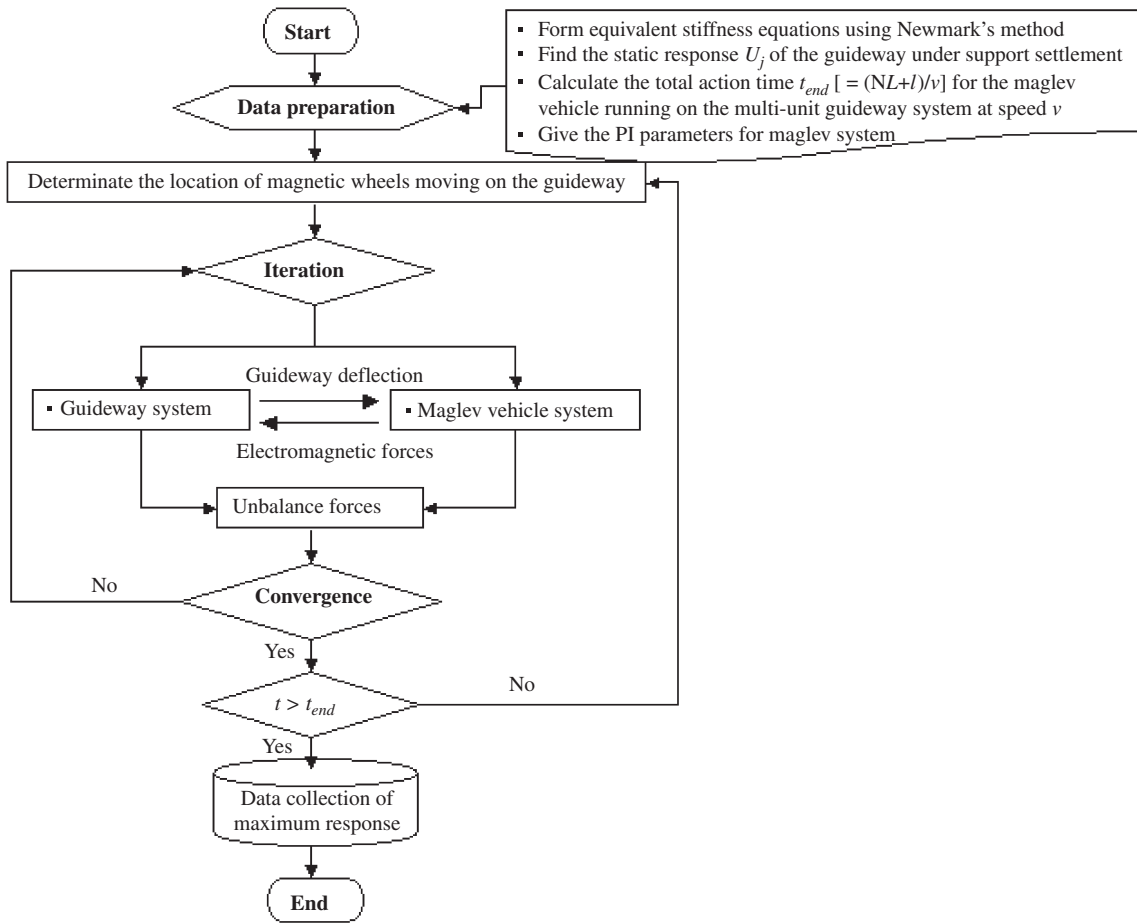
Fig. 4. Flow chat of incremental-iterative procedure.

6. Numerical examples

Fig. 2 shows a maglev vehicle suspended by multiple magnets is crossing a series of simply supported guideway girders at constant speed v. The properties of the guideway and maglev vehicle are listed in Tables 1 and 2, respectively. It was well known that if the *acceleration response*, rather than the displacement response, of a structure is of concern, the contribution of higher modes has to be included in the computation [16–18]. From the convergent verification of computed results for a suspended beam with simple supports presented in Ref. [19], the first 20 modes of shape functions in Eq. (22) are sufficient to compute the acceleration response of a simple beam. And the time step of 0.001 s and the ending time of $t_{\mathrm{end}} = (NL+l)/v$ are employed to compute the interaction responses of the maglev vehicle/guideway system. Here, N is the total span number of the multi-unit guideway.

In addition, to account for the random nature and characteristics of guide-rail irregularity in practice, the following *power spectrum density* (PSD) function [21] is given to simulate the vertical profile of track geometry variations:

$$S(\Omega) = \frac{A_v \Omega_c^2}{(\Omega^2 + \Omega_r^2)(\Omega^2 + \Omega_c^2)}, \tag{27}$$

where Ω is the spatial frequency, and A_v ($= 1.5 \times 10^{-7}$ m), Ω_r ($= 2.06 \times 10^{-6}$ rad/m), and Ω_c ($= 0.825$ rad/m) are relevant parameters. Fig. 5 shows the vertical profile of track irregularity [20] for the simulation of rail geometry variations in this study.

Table 1
Properties and natural frequencies of the guideway.

L (m)	EI (kN m^2)	m (t/m)	c (kN-s/m)	f_1 (Hz)	f_n [a] (Hz)
25	2.5×10^7	3.76	15.4	6.5	$4n^2$

[a] f_n is the nth natural frequency of a simple beam.

Table 2
Properties of the maglev vehicle.

l (m)	K	m_b (kg/m)	m_v (kg/m)	m_w (kg)	c_v (Ns/m/m)	k_v (N/m/m)	i_0 (A)	R_0 (Ω)
25	8	1200	600	500	4.1×10^3	7.5×10^3	25	1.0
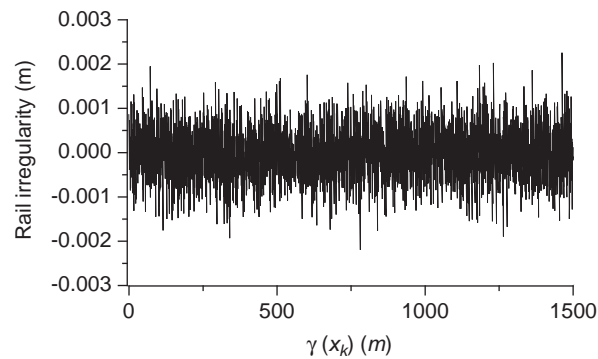
Fig. 5. Rail irregularity (vertical profile).

6.1. Numerical verification

Prior to investigating the dynamic response of the maglev vehicle/guideway system subject to ground settlement, a TR06 maglev vehicle model referred to Ref. [6] is selected to simulate its dynamic behavior running on a concrete guideway girder. The main data for the TR06 maglev vehicle with car length of 24 m and a single-span concrete guideway with span length of 24.854 m [6,14] are given as follows: $EI = 24.56 \times 10^6$ kN m^2, $m = 3760$ kg/m, $m_v = 1.5$ t/m, $m_b = 1.4$ t/m, $c_v = 4.5$ kN s/m/m, $k_v = 20$ kN/m/m, $h_0 = 8$ mm, $i_0 = 37$ A, and $R_0 = 1.1 \Omega$. Let the maglev vehicle travel on the *smooth* guideway with a constant speed of 400 km/h. Considering the PI parameters of ($K_p = 0.17$, $K_i = 0.15$), the time history responses of the mid-span guideway deflection and the midpoint acceleration of the car body, together with the numerical results referred to Refs. [6,20], have been plotted in Figs. 6 and 7, respectively. They indicate that the proposed vehicle/guideway model has the ability to simulate the dynamic behavior of a TR06 maglev vehicle running on a concrete guideway even though the present acceleration response of car body exists a phase difference in vibration compared with that given in Ref. [6]. The reason of phase difference is attributed to: (1) from the equations of motion in terms of *midpoint* vertical displacements (u_v, u_b) in Eqs. (8a) and (9a), it can be regarded as a 2-dof system; (2) due to the coupling nature of a 2-dof system, its response appears a significant phase difference in *vertical* vibration compared with that of one vertical-dof car body given in Ref. [6].

6.2. Application of the Z–N tuning rule

With the same initial control voltage $R_0 i_0$ for the maglev suspension system, two desired levitation gaps are respectively used for the maglev vehicle model, i.e., $h_0 = 0.015$ and 0.03 m. They are named MG-1 and MG-2,
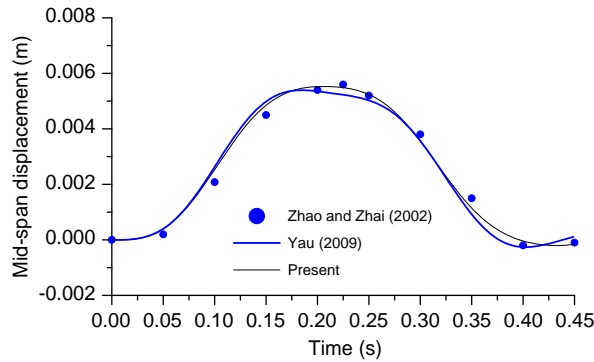
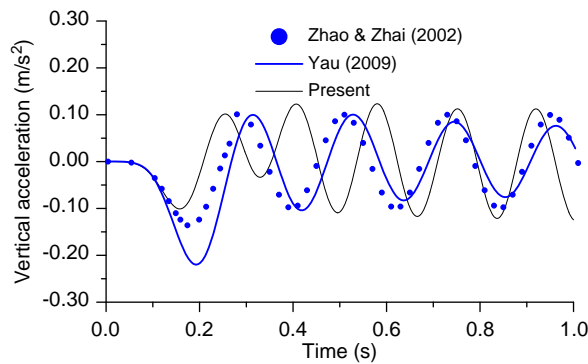Fig. 6. Time history response of mid-span displacement.

Fig. 7. Time history response of vertical acceleration for the maglev vehicle.

respectively. From the numerical results presented in Ref. [20], a neuro-PI controller is available to control the dynamic response for a row of maglev oscillators moving on a guideway. Thus, in the following numerical examples, a PI controller based on Z–N tuning rule will be also employed to tune the electromagnetic force $G_k(i_0, h_0)$ in the maglev system. The Z–N tuning rules [9,10] have been proved very useful in determining the optimal parameters of a PI controller in process control system, from which the PI parameters are given by $K_p = 0.45K_{cr}$ and $K_i = 0.54K_{cr}/T_{cr}$. Here K_{cr} means the critical proportional gain of the PI controller by increasing only the proportional control action (i.e., $K_i = 0$) K_p from 0 to a critical value K_{cr} so that the output first exhibits an oscillation behavior with a critical period T_{cr} [10]. In the present example, the PI tuning parameters are first determined using the Z–N tuning rule and then the interaction responses of the maglev vehicle and guideway are computed.

For the purpose of demonstration, let the maglev vehicle supported with *eight* magnetic wheels cross a single span guideway at an extreme speed 600 km/h. By trials for different K_p to reach the critical parameter K_{cr}, the corresponding time history responses of the control error e_1/γ_0 for the MG-1 and MG-2 to oscillate have been plotted in Fig. 8. They show that the critical period of the control error function for the maglev vehicle increases along with the increase in levitation gap. The transient responses of middle vertical acceleration of the rigid car body and the guideway have been depicted in Figs. 9 and 10, respectively. As shown in Fig. 9, the response amplitude of MG-2 is generally larger than that of MG-1, since a large air gap in a maglev system may allow the magnetic wheels to oscillate with a larger amplitude, from which the vibrating rigid levitation frame would directly excite the car body through the interaction layer (a distributed spring–dashpot system) and then the maglev vehicle's response was amplified as well. The time history responses plotted in Fig. 11 for the midpoint acceleration of the levitation frame with the desired air gaps can verify this phenomenon. The simulation results indicate that a maglev vehicle with larger desired levitation gap requires more proportional gain to restrict its magnetic wheels to oscillate within around a chosen nominal operating point. Table 3 gives the corresponding optimal PI parameters for the maglev vehicles of MG-1 and M-2 based on Z–N tuning rule.
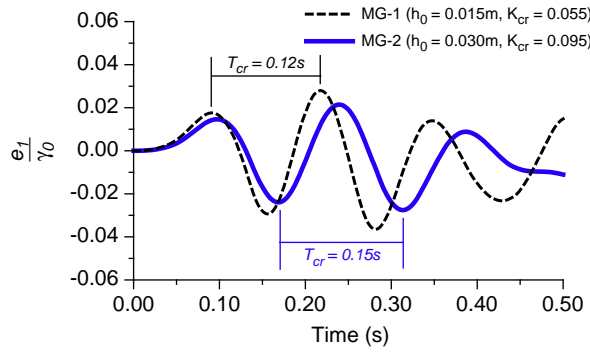
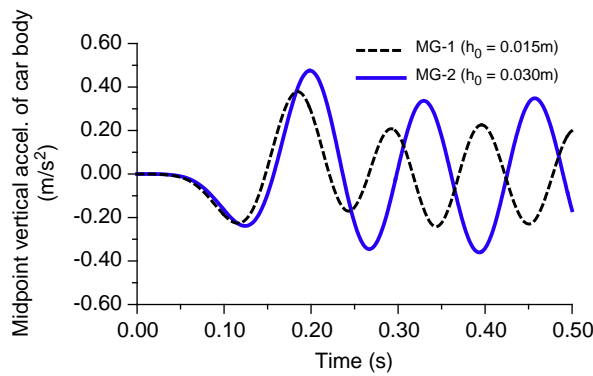Fig. 8. Transient oscillation with a critical period T_{cr}.

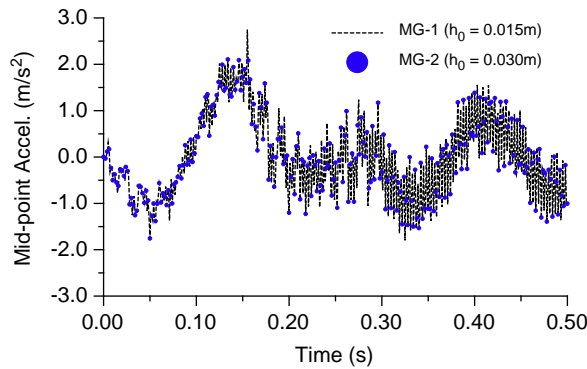Fig. 9. Vertical acceleration of midpoint of the car body.

Fig. 10. Response of mid-span acceleration of the guideway.

On the other hand, Fig. 10 shows that the acceleration responses of the guideway caused by the traveling maglev vehicles of MG-1 and MG-2 are almost identical due to the fact that the effects of inertia and levitation gaps of the moving maglev vehicle are generally small on the guideway response. This conclusion is consistent with that presented in Refs. [2,20].

6.3. Maximum response analysis of maglev vehicles

In the following examples, the maglev vehicle model listed in Table 2 is used to travel over a series of guideway girders with twelve spans ($N = 12$) at constant speed ranging from 100 to 700 km/h, respectively.
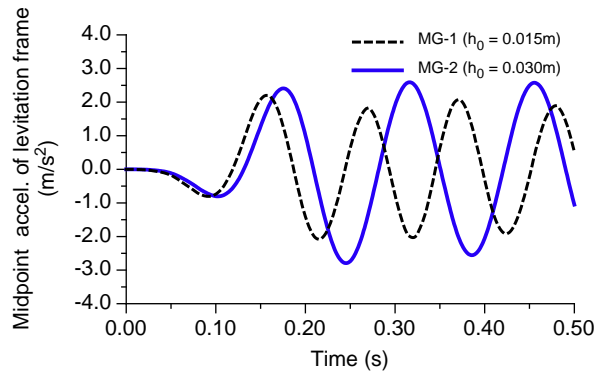
Fig. 11. Midpoint acceleration of the levitation frame.

Table 3
PI parameters based on Z–N tuning rule for the critical gain K_{cr} and critical period T_{cr}.

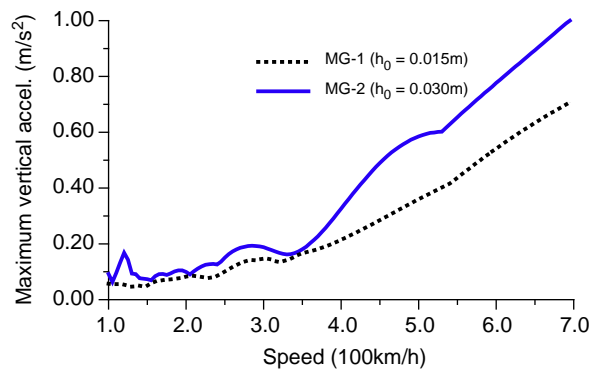| Type	h_0 (m)	K_{cr}	T_{cr} (s)	K_p ($= 0.45K_{cr}$)	K_i ($= 0.54K_{cr}/T_{cr}$)
MG-1	0.015	0.055	0.12	0.025	0.25
MG-2	0.030	0.095	0.15	0.043	0.34

Fig. 12. $a_{v,\max}-v$ plot of the maglev vehicle.

Considering the optimal PI parameters in Table 3 proposed by Z–N tuning rule obtained from Section 6.2, the maximum vertical acceleration ($a_{v,\max}$) of the rigid car body has been plotted in Fig. 12 against speed. Such a relationship is denoted as $a_{v,\max}-v$ plot in the following. As can be seen from the acceleration amplitudes plotted in Fig. 12, the maglev vehicle MG-2 is generally larger than the vehicle MG-1. It means that the magnetic wheels at levitation frame of MG-2 might experience more intensive oscillation due to its larger air gap. In addition, the $a_{v,\max}-v$ plot in Fig. 12 shows that the maximum acceleration of the maglev vehicle increases along with the increase of running speeds. In addition, Fig. 13 depicts the corresponding maximum response ($a_{\max}$) of midspan acceleration at the departure guideway girder under the action of MG-1 and MG-2, respectively. The results show that the $a_{\max}-v$ plots for the moving MG-1 and MG-2 are almost identical as the speed is lower than 600 km/h. The reason is that the inertial force induced by the running maglev vehicle acting on the guideway girder is much smaller than the *static* weight of the vehicle. However, once the running speed exceeds 600 km/h, a significant difference of $a_{\max}-v$ plots for both MG1 and MG-2 appears since the maximum acceleration amplitudes for MG-2 rather approximate 1 m/s² in the corresponding $a_{v,\max}-v$ plot of
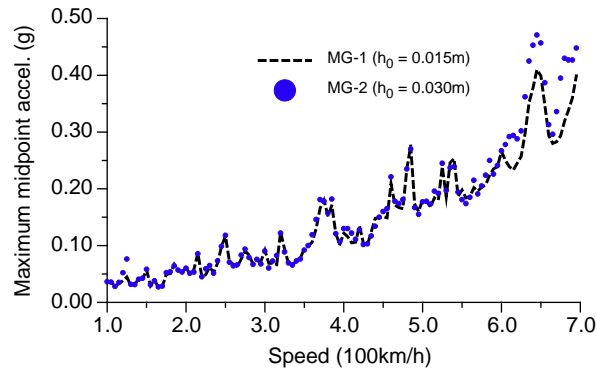
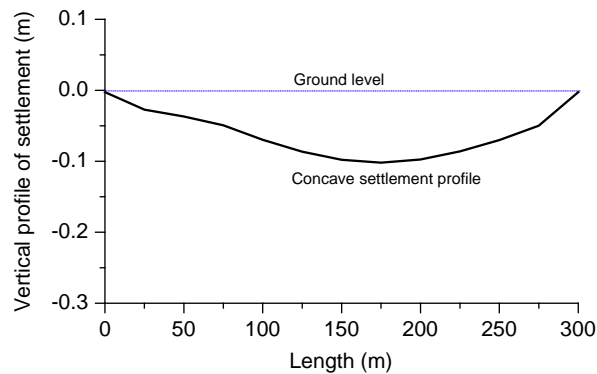Fig. 13. $a_{max}-v$ plot of the departure span of the guideway.

Fig. 14. Vertical profile of ground settlement.

Fig. 12. It means that the inertial effect of the maglev vehicles moving over 600 km/h becomes quite significant on the guideway response.

6.4. Effect of ground settlement

A possible reason of regional land subsidence may be caused by over groundwater utilization for agricultural and fishery farming use. To take into account the influence of ground settlement on the interaction response of maglev vehicle/guideway system, the concave-type settlement profile with a maximum settlement of 0.1 m shown in Fig. 14 is employed to simulate the regional land subsidence along the guideway route. With the same properties of guideway units and maglev vehicles given in Section 6.2, Fig. 15 shows the analysis results for the $a_{max}-v$ plot of the departure span of the guideway system. It indicates that the influence of differential settlement on the guideway response are generally insignificant since a simple beam subject to support movements merely experiences a rigid body displacement or rotation (see Eq. (19)), from which there is no additional natural deformation occurring in the beam. On the other hand, Fig. 16 depicts the $a_{v,max}-v$ plots for the maglev vehicles of MG-1 and MG-2, respectively. Generally, the inclusion of ground settlement may amplify the acceleration amplitude of the moving maglev vehicles, especially for the speeds higher than 450 km/h. But the amplified extent of acceleration amplitudes for MG-2 is significantly smaller than that for MG-1. The reason is that the desired levitation gap (30 mm) of MG-2 has more capacity to cover the additional guideway deflections due to ground support settlement.
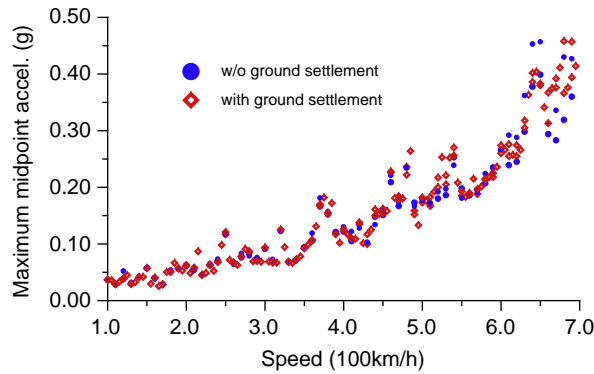
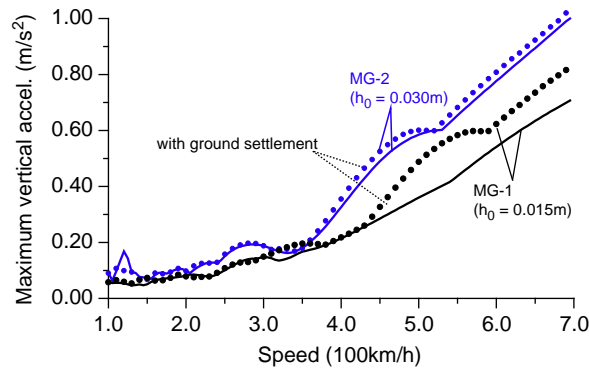Fig. 15. Effect of ground settlement on $a_{max}-v$ plot of the departure span.

Fig. 16. Effect of ground settlement on $a_{v,max}-v$ plot of the maglev vehicle.

7. Concluding remarks

In this study, a rigid double-beam system suspended by a number of equal-distant electromagnetic forces is developed to model a maglev vehicle supported with multiple magnets, in which an on-board PI controller based on Z–N tuning rule makes available to tune the electromagnetic forces around a specific nominal desired levitation gap. To investigate the influence of ground settlement on the interaction response of the maglev vehicle/guideway system, a *decomposition* method is used to extract the *static* displacement from the total response of the guideway girder undergoing support settlement. Then the nonlinear dynamic response analysis of the maglev vehicle/guideway system has been carried out by Galerkin's method and computed using an iterative approach with Newmark's finite difference formulas. From the numerical studies, the following conclusions are reached:

(1) Considering the PI controller with *constant* tuning gains based on Z–N method, the maximum acceleration of a maglev vehicle generally increases along with the increase in moving speeds.
(2) The dynamic response of the maglev vehicle with larger levitation gap is generally larger than that with smaller one since its magnetic wheels attached to levitation frame might experience more intensive oscillation within larger air gap.
(3) Both the inertial effect of moving maglev vehicle and the influence of ground settlement are generally small on the guideway response. But as the maglev vehicle travels over the guideway at very high speeds, the effect of inertial force of the vehicle will become rather significant on the guideway response.
(4) The amplified extent of $a_{v,max}-v$ plot for the maglev vehicle MG-2 running on the guideway system with support settlement is insignificant in that its desired levitation gap (30 mm) has more capacity to cover the additional guideway displacement due to support settlement.

(5) The acceleration amplitude of the maglev vehicle with smaller levitation gap (MG-1) is significantly affected by the presence of ground support settlement. Such a fact should be taken into account in aligning the maglev transportation route that has to cross the region with potential local land subsidence.

(6) In this study, the PI controller with *constant* tuning gains for controlling the maglev system is selected to investigate the amplification effect of ground settlement on the maglev vehicle/guideway system. However, the maximum vertical acceleration response of a running maglev vehicle is generally restricted within 0.02–0.05 g for ride quality and maneuverability [2]. Thus a future research can be focused on the development of a controller with speed-related tuning gains to regulate the electromagnetic forces in maglev system so that the vehicle's response can satisfy such a strict limitation.

(7) As the moving speed of a maglev vehicle coincides with or exceeds the Rayleigh wave velocity of soft soil [22], guideway–soil interaction will become significant and affect the electromagnetic force in maglev system due to its motion-dependent nature. Thus, a further study can be conducted to introduce the guideway–soil interaction into the maglev vehicle/guideway system.

Appendix A

The mass, damping, and stiffness matrices for the maglev vehicle model are given as follows:

$$[m_c] = \begin{bmatrix} \begin{bmatrix} m_b + K m_w/l & 0 & 0 & 0 \\ & I_{bT} & 0 & 0 \\ & & m_v & 0 \\ \text{symm.} & & & I_v \end{bmatrix}_{4\times4} & [0]_{4\times K} \\ [0]_{K\times4} & \begin{bmatrix} \Gamma_0 & 0 & 0 \\ 0 & \ddots & 0 \\ 0 & 0 & \Gamma_0 \end{bmatrix}_{K\times K} \end{bmatrix}, \tag{A.1}$$

$$[c_c] = \begin{bmatrix} \begin{bmatrix} c_v & 0 & -c_v & 0 \\ & \dfrac{c_v l^2}{12} & 0 & -\dfrac{c_v l^2}{12} \\ & & c_v & 0 \\ \text{symm.} & & & \dfrac{c_v l^2}{12} \end{bmatrix}_{4\times4} & [0]_{4\times K} \\ -R_0\gamma_0\begin{bmatrix} 1 & d_1 & 0 & 0 \\ \vdots & \vdots & \vdots & \vdots \\ 1 & d_K & 0 & 0 \end{bmatrix}_{K\times4} & \begin{bmatrix} K_p + R_0 h_1 & 0 & 0 \\ 0 & \ddots & 0 \\ 0 & 0 & K_p + R_0 h_K \end{bmatrix}_{K\times K} \end{bmatrix}, \tag{A.2}$$

$$[k_c] = \begin{bmatrix} \begin{bmatrix} k_v & 0 & -k_v & 0 \\ & \dfrac{k_v l^2}{12} & 0 & -\dfrac{k_v l^2}{12} \\ & & k_v & 0 \\ \text{symm.} & & & \dfrac{k_v l^2}{12} \end{bmatrix}_{4\times4} & 2\dfrac{f_0}{\gamma_0}\begin{bmatrix} 1 & \cdots & 1 \\ d_1 l/K & \cdots & d_K l/K \\ 0 & \cdots & 0 \\ 0 & \cdots & 0 \end{bmatrix}_{4\times K} \\ [0]_{K\times4} & \begin{bmatrix} K_i + R_0\dot{h}_1 & 0 & 0 \\ 0 & \ddots & 0 \\ 0 & 0 & K_i + R_0\dot{h}_K \end{bmatrix}_{K\times K} \end{bmatrix}, \tag{A.3}$$

and the displacement and force vectors are respectively expressed as

$$\{u_v\} = \begin{Bmatrix} u_b \\ \theta_b \\ u_v \\ \theta_v \\ \{e_k\}_{K\times 1} \end{Bmatrix}, \quad \{f_v\} = \begin{Bmatrix} \dfrac{f_0}{K\gamma_0^2}\sum_{k=1}^{K}e_k^2 \\ \dfrac{f_0 l}{K\gamma_0^2}\sum_{k=1}^{K}[d_k e_k^2] \\ 0 \\ 0 \\ \{R_0\gamma_0(\dot{r}-\dot{u}_j)|_{x=x_k}\}_{K\times 1} \end{Bmatrix}. \tag{A.4,5}$$

Acknowledgements

References

[1] A. Bittar, R.M. Sales, H$_2$ and H$_\infty$ control for maglev vehicles, *IEEE Control Systems Magazine* 18 (4) (1998) 18–25.
[2] Y. Cai, S.S. Chen, D.M. Rote, H.T. Coffey, Vehicle/guideway dynamic interaction in maglev systems, *Journal of Dynamic Systems, Measurement, and Control* 118 (1996) 526–530.
[3] Y. Cai, S.S. Chen, Dynamic characteristics of magnetically levitated vehicle systems, *Applied Mechanics Reviews* 50 (11) (1997) 647–670.
[4] X.J. Zheng, J.J. Wu, Y.H. Zhou, Numerical analyses on dynamic control of five-degree-of-freedom maglev vehicle moving on flexible guideways, *Journal of Sound and Vibration* 235 (2000) 43–61.
[5] X.J. Zheng, J.J. Wu, Y.H. Zhou, Effect of spring non-linearity on dynamic stability of a controlled maglev vehicle and its guideway system, *Journal of Sound and Vibration* 279 (2005) 201–215.
[6] C.F. Zhao, W.M. Zhai, Maglev vehicle/guideway vertical random response and ride quality, *Vehicle System Dynamics* 38 (3) (2002) 185–210.
[7] J.D. Yau, L. Fryba, Response of suspended beams due to moving loads and vertical seismic ground excitations, *Engineering Structures* 29 (2007) 3255–3262.
[8] J.D. Yau, Vibration of arch bridges due to moving loads and vertical ground motions, *Journal of Chinese Institute of Engineers* 29 (2006) 1017–1027.
[9] K.J. Astrom, T. Hagglund, *Automatic Tuning of PID Controllers*, Instrument Society of America, 1988.
[10] K. Ogata, *Modern Control Engineering*, third ed., Prentice-Hall, Englewood Cliffs, NJ, 1997.
[11] E. Poulin, A. Pomerleau, PI settings for integrating processes based on ultimate cycle information, *IEEE Transactions on Control Systems Technology* 7 (4) (1999) 509–511.
[12] N.M. Newmark, A method of computation for structural dynamics, *Journal of Engineering Mechanics Division* 85 (1959) 67–94.
[13] D.L. Trumper, S.M. Olson, P.K. Subrahmanyan, Linearizing control of magnetic suspension systems, *IEEE Transactions on Control Systems Technology* 5 (4) (1997) 427–438.
[14] G. Bohn, G. Steinmetz, The electromagnetic levitation and guidance technology of the Transrapid test facility Emsland, *IEEE Transactions on Magnetics* 20 (5) (1984) 1666–1671.
[15] P.K. Sinha, *Electromagnetic Suspension, Dynamics and Control*, Peter Peregrinus Ltd., London, UK, 1987.
[16] J.D. Yau, Y.B. Yang, Vertical accelerations of simple beams due to successive loads traveling at resonant speeds, *Journal of Sound and Vibration* 289 (2006) 210–228.
[17] J.D. Yau, Vibration of parabolic tied-arch beams due to moving loads, *International Journal of Structural Stability and Dynamics* 6 (2006) 193–214.
[18] J.D. Yau, Train-induced vibration control of simple beams using string-type tuned mass dampers, *Journal of Mechanics* 23 (4) (2007) 329–340.
[19] J.D. Yau, Y.B. Yang, Vibration of a suspension bridge installed with a water pipeline and subjected to moving trains, *Engineering Structures* 30 (2008) 632–642.
[20] J.D. Yau, Vibration control of maglev vehicles traveling over a flexible guideway, *Journal of Sound and Vibration* 321 (2009) 184–200.
[21] Y.B. Yang, J.D. Yau, Y.S. Wu, *Vehicle–Bridge Interaction Dynamics*, World Scientific, Singapore, 2004.
[22] A.V. Metrikine, K. Popp, Vibration of a periodically supported beam on an elastic half-space, *European Journal of Mechanics A/Solids* 18 (4) (1999) 679–701.